This is the accepted version of:

Radrizzani, M., et al. "Aptamer-quantum dots platform for SARS-CoV-2 viral particle detection by fluorescence microscopy." International Journal of Biological Macromolecules 278 (2024): 134839.

https://doi.org/10.1016/j.ijbiomac.2024.134839

Aptamer-Quantum Dots platform for SARS-CoV-2 viral particle detection with a fluorescence microscope

M. Radrizzani^a*, C. Y. Flores^b, J. Stupka^c, C. D'alessio^d, O. Garate^e, L.J. Mendoza Herrera^f, A.A. Castello^g, J. S. Yakisich^b, C. Perandones^f and M. Grasselli^b*

- ^a Neuro and Molecular Cytogenetics Laboratory. Institute of Emerging Technologies and Applied Sciences (ITECA) - National Council for Scientific and Technical Research (CONICET) and School of Science and Technology, National University of San Martín, Av. Gral. Paz 5445, San Martín B1650WAB, Argentina.
- Laboratorio de Materiales Biotecnológicos (LaMaBio), Departamento de Ciencia y Tecnología, Universidad Nacional de Quilmes. GBEyB, Grupo Vinculado IMBICE-CONICET, Roque Sáenz Peña 352, Buenos Aires B1876BXDI, Argentina.
- c INEI-ANLIS, Ministry of Health, Buenos Aires, Argentina.
- Facultad de Ciencias Exactas y Naturales, Departamento de Fisiología y Biología Molecular y Celular, Instituto de Biociencias, Biotecnología y Biología Traslacional (iB3), Ciudad Universitaria-Pabellón II, Buenos Aires 1428, Argentina
- Nanomateriales Funcionales, INTI-Micro y Nanotecnología, Instituto Nacional de Tecnología Industrial, San Martín B1650, Argentina
- f Centro de Investigaciones Ópticas (CIOp),(CONICET La Plata-CIC), Gonnet, Buenos Aires, Argentina.
- Laboratorio de Inmunología y Virología (LIV), Departamento de Ciencia y Tecnología, Universidad Nacional de Quilmes. Roque Sáenz Peña 352, Buenos Aires B1876BXDI, Argentina.
- Department of Pharmaceutical Sciences, School of Pharmacy, Hampton University, Hampton, VA
 23693, USA.
- National Administration of Laboratories and Health Institutes of Argentina (ANLIS) Dr. Carlos G. Malbrán, Buenos Aires, Argentina
- * Co-corresponding authors

E-mail addresses: mariano.grasselli@unq.edu.ar; martin.radrizzani@gmail.com

Abstract

The virus is the smallest known replicative unit, usually in nanometerrange sizes. The most simple and sensitive detection assay involves molecular amplification of nucleic acids. This work shows a novel, straightforward detection assay based on the interaction of viral particles with fluorescent nanoconstructs without using enzymatic amplification, washing or separation steps.

Fluorescent nanoconstructs are prepared with individual quantum dots of different emitting fluorescence, green and red, as a core. They are decorated with aptamers developed to recognise the receptor-binding region of the SARS-CoV-2 spike protein.

Nanoconstructs can recognise SARS-CoV-2 viral particles fixed onto a coverglass generating aggregates. Meanwhile, SARS-CoV-2 viral particles/nanoconstructs complexes in solution yield macroaggregates, which can be visualised by a fluorescence microscope at low magnification.

The method takes advantage of the enhanced affinity of homomultivalent interactions and light fluorescence signal amplification of quantum dots. The multiple molecular recognition allowed the detection of SARS-CoV-2 viral particles from a few microliters of patient swabs. This specific SARS-CoV-2/nanoconstructs interaction generates insoluble and precipitating aggregates. By using a mixture of green and red fluorescent nanoconstructs, upon the viral particle interaction at a distance closer than 250 nm, they yield yellow fluorescence, which is easily identifiable by a fluorescence microscope. This is a consequence that they do not comply with the Rayleigh criterion, and in this way, washing and separation steps are not required. In addition, the larger size of aggregates allows one to easily recognise them at low magnification (200x), offering a sensitive, simple, and cheap alternative for viral detection.

Keywords: Aptamers; quantum dots; SARS-CoV-2; viral detection; nanoparticles; multivalent.

1. Introduction

Molecular methods and lateral flow assays (LFA) have been widely used during the last pandemia to detect and control viral dissemination. Molecular analysis based on the polymerase chain reaction (PCR) and its isothermal version, the loop-mediated isothermal amplification reaction, were broadly used due to the high sensitivity. However, these tests suffer from a complex assay workflow and several specific reagents and equipment, contributing to their high cost and extended analysis time. Meanwhile, LFA methods allow direct detection of protein antigens in a shorter time, reaching a direct ratio to antigen amount. They suffer from lower sensitivity; however, it is not always true in the case of viral detection of enveloped viruses. It can be partially compensated by the large number of antigens per virion particle. However, the low viral amounts could yield false negative results [Niguyen et al., 2020].

The core of any bioassay is the recognition molecule. In most of them, antibodies are the preferred molecules used. However, selecting polyclonal or monoclonal antibodies with specific biorecognition properties requires the complex biological machinery of mammalian cells [Wiberg et al., 2006]. Instead, synthetic antibodies, called aptamers, have been proposed as a recognition tool [Jayasena, 1999; Lee et al., 2006]. Aptamers are synthetic DNA or RNA single or double-stranded oligonucleotides with sizes ranging from 10 to 100 nucleotides and recognise a selected target [Chakraborty et al., 2022]. The aptamers were described more than 30 years ago [Tuerk and Gold, 1990; Ellington and Szostak, 1990]; however, they have recently attracted more attention as a consequence of their technological features, such as short development period, higher stability, highly resistant to degradation, and a straightforward manufacturing process [Chakraborty et al., 2022].

Much effort has been made to move further to single-detection molecule systems since the new millennium. Individual molecules have been detected using two-colour coincident fluorescence events. These methods allow quantitatively measuring protein analytes at the femtomolar level [Li et al., 2004]. This technology, which uses a microfluidic channel integrated into advanced fluorescence microscopy and luminescent quantum dots (QDs), can

provide ultrasensitive detection of molecules without the involvement of any enzymatic amplification [Agrawal et al., 2006; Zhou et al., 2013]. In this way, some drawbacks related to molecular analysis can be overcome. However, sophisticated and high-cost detection instruments and data processing are required for their application.

QDs have outstanding brightness, simplicity of excitation, and photostability. These enhanced fluorescence properties of QDs can replace the amplification step performed by enzymatic reactions in molecular diagnostics and ELISA [Agrawal et al., 2006]. In addition, using dual-colour detection, washing, and separation steps are not necessarily performing the analysis in a homogeneous phase [Agrawal et al., 2006]. These features can revolutionise analytical chemistry by changing current conventional technologies, based on intensity-determined measurements, by processes based on single-molecule counting [Song et al., 2013; Hu et al., 2017].

Recently, a single-molecule homogeneous immunoassay has been reported by counting spatially "overlapping" two-colour QDs using a wide-field fluorescence microscope [Liu et al., 2018]. However, in this technique, a relatively high concentration of QDs, decorated with capture and detection antibodies, should be used.

In recent years much effort from the scientific community has been applied to develop QDs prepared from other elements to improve their technological properties to be useful for diagnosis, such as water solubility, lower toxicity, and/or tuning the plasmonic signal [Tyrakowski and Snee, 2014]. Also, straightforward and low-cost chemical procedures to prepare them have been published [Almendral-Parra et al., 2014].

QDs solubility in complex biological media was one of the technical issues allowing these outstanding nanomaterials to be used in a natural milieu. Recently, albumin multilayer coating procedures were described for preparing biohybrid nanoconstructs containing a core of inorganic nanoparticles [Achilli et al., 2022; Traverso et al., 2023], which showed a shallow 'corona effect' under in vitro cell culture conditions and allowed an enhanced cell uptake under near-physiological conditions. Using QDs as a core, it could track single

particles in cell cytoplasm using an epifluorescence microscope [Traverso et al., 2023].

Considering the advanced biocompatible properties of these biohybrid QDs (Bioh-QDs) nanostructures, in this work, they are applied to detect single SARS-CoV-2 viral particles in swab samples. Specific aptamers are selected to decorate Bioh-QDs to interact specifically with viral particles. These nanoconstructs generate fluorescent aggregates in the presence of SARS-CoV-2 viral particles, which are easily visualised by changes in the colour fluorescence emission without washing, separation or amplification steps.

2. Materials and Methods

QDs solutions at 5 mg/ml (1.0 nmol/mg) with emission wavelengths at 525 nm and 630 nm, corresponding to green (Catalog#: QD-525-A-5MG) and red (Catalog#: QD-630-A-5MG) fluorescence emissions respectively, were purchased from Cytodiagnostics Inc. (Burlington, Canada). Human serum albumin (HSA, 200 mg/mL) was donated from the Laboratorio de Hemoderivados, Universidad Nacional de Córdoba (Córdoba, Argentina). All other reagents were analytical grade.

2.1 Spike Receptor-Binding domain preparation

Spike Receptor-Binding Domain (RBD) protein fragment was produced in recombinant *Pichia past*oris. Fermentations were carried out in a stirred-tank bioreactor (BioFlo 115, New Brunswick Scientific; Edison, NJ, USA) using a four-stage procedure and purified by NTA-Ni⁺² chromatography column [Noseda et al., 2023].

2.2 Aptamer selection

Aptamer was selected according to the previously described procedure [Moncalero et al., 2011]. Briefly, synthetic aptamer library (5'-CGGAATTCCGAGCGTGGGCGT (N)50 TACGCCCACGCTCGAG-3' (87 mer)), (GBT, Argentina) was amplified at 1 μ M concentration using 2 μ M of each primer (primer fw: 5'-CGGAATTCCGAGCGTGGGCGT-3'; and primer rev: 5'-CTCGAGCGTGGGCGTA -3') applying 25 cycles of PCR (94°C for 30 s, 58°C for 30

s, 72°C for 10 s steps). PCR products were purified by ethanol 70% precipitation method and resuspended in PBS. Previously incubated dsDNA is heated at 95 °C for 5 min and then cooled at 4 °C in two volumes of PBS-BSA 5% to yield ssDNA chains. This product (50 μ g) was incubated with RBD (10 μ g) in the final volume of 100 μ l (in quadruplicate) for 30 min. The mixture is filtered by a nitrocellulose membrane and washed with PBS (three times). Aptamers bound to the targets were eluted by heating the membrane at 95°C for 5 min in milliQ-filtered water (50 μ l). Eluted aptamers were used as a template to be amplified by PCR. Aptamer selections with recognition properties were cloned into the pGEM-T easy vector (Promega) and sequenced.

2.3 Aptamer labelling

Selected aptamers were amplified by PCR of one mL of final volume using a forward primer containing one of the following tags: 5'-C6-NH₃ and 5' DNAzymes peroxidase [Longinotti et al., 2021]. The final product is purified by 70 % ethanol precipitation. Pellet was resuspended in water and quantified by UV-spectroscopy (Nanodrop 1000).

2.4 Preparation of water-soluble QDs

The water-soluble QDs were obtained by a procedure similar to the one described [Traverso et al., 2023]. Briefly, commercial QDs suspension (20 μ L) was diluted in chloroform: methanol (4:1) (1 mL) followed by gently adding an aqueous phase prepared with PBS (350 μ L) + HSA (10 mg/ml, 350 μ L) + glutaraldehyde (5%, 1.5 μ L) + water (298.5 μ L). The mixture was sonicated using a SONICS Vibra Cell VCX50 ultrasonicator until the solution reached 60 °C. The suspension was centrifuged at 10,000 g for a few seconds to separate and recover the upper water phase containing the QDs (gluta-QDs). QDs of different emission fluorescence are prepared separately.

2.5 Decoration of Apt-QDs

Gluta-QDs were added to the aptamer solution (150 μ g/50 μ L) in PBS up to 1 mL and incubated at room temperature overnight (ON) with head-tail agitation. The remaining reactive sites were blocked by adding 10% Tris-Glycine 1 M, pH 8.8 solution for 1 h. These decorated Bioh-QDs with Apt (Apt-QDs) were recovered by centrifugation at 10,000 g for 15 min. The supernatant

was discarded, and Apt-QDs were resuspended in 500 μ l milliQ H₂O. The suspension was measured by UV-spectroscopy (Nanodrop 1000), and a 260/280 ratio was determined. Visualisation under Ultraviolet Light C (350 nm) was used as a quality control to monitor the preservation of the fluorescence emitted by the QDs in the nanoconstruct after each preparation.

2.6 Filter binding assay

The recognition of the DNA aptamers to their respective targets was analysed by incubation RBD (1 µg) and DNAzyme-peroxidase aptamer (0 to 500 ng) in the final volume of 100 µl for 30 min. The mixture is filtered by a nitrocellulose membrane (BioRad Dot blot system) and washed with PBS (three times). Aptamers bound to the targets were incubated with TKT buffer (Tris-HCl 25 mM pH 8, KCl 20 mM, NaCl 200 mM, Triton X-100 0.05%, dimethyl-sulfoxide 0.1%) and developed with luminol system (SuperSignal™ West Pico PLUS Chemiluminescent Substrate. Thermo Scientific™). Images were recorded using the ImageQuant LAS 500 (GE Healthcare Life Sciences).

2.6 Characterisation de decorated Bioh-QDs

UV-vis spectroscopy of Bioh-QDs was performed in Nanodrop 1000. Bioh-QDs were analysed by electrophoresis on low melting Agarose gel 0.8%, using 0.5x TBE buffer. Fluorescamine (FSC) 1% and ethidium bromide (EtBr) to detect proteins and DNA, respectively.

Diluted suspensions of Bioh-QDs were fixed with glutaraldehyde 0,7% for 30 min and stained with uranyl acetate, and analysed in a Zeiss EM 109-T Transmission Electron Microscope (TEM) equipped with a Gatan ES1000W digital camera at the Instituto de Biología Celular y Neurociencia, LANAIS-MIE (UBA-CONICET).

Hydrodynamic diameters of nanoconstructs were measured on 100 μ l diluted samples by Dynamic Light Scattering (DLS) in the Wyatt Dyna-Pro reader and analysed with the Dynamics Software v7.8. Between 500,000 and 2,000,000 events (10 acquisitions, five s/each) were studied at 25 °C.

Dot blot was performed by seeding RBD (1 μg) on nitrocellulose membrane, blocked with PBS-BSA 5% and filtered with Apt#9-QDs (green and

red ones). Fluorescence signals were recorded using the ImageQuant LAS 500 (GE Healthcare Life Sciences) and Olympus X71 epifluorescence microscope using a 488 nm/543 nm/dual filter, respectively.

2.8 SARS-CoV-2 recognition by Apt#9-QDs

The SARS-CoV-2 viral sample (1.5 μ L) was seeded in a 15 mm² microwell onto a coverslip and dried at RT for 60 min. Two μ L of mixed with green and red Apt#9-QDs mixture 1 nM were added and dried at RT. The microwell was visualised by Olympus X71 epifluorescence microscope at 1600x magnification (1000x plus 1,6 magnifying glass), using a 488 nm/543 nm/dual filter.

2.7 SARS-CoV-2 detection in swab samples

SARS-CoV-2 viral samples were tested for SARS-CoV-2 using lateral flow detection kit Abbott BinaxNOW COVID-19 Self Test from 12 patient swabs. Twelve positive and negative patient swabs were collected in the Hospital General de Agudos "Parmenio Piñero" and stored at 4 °C. All the samples were centrifuged for 10 minutes at 10.000 rpm to avoid tissue or insoluble particles from the swab samples.

2.7.1 Detection of single SARS-CoV-2 viral particles

One and a half microliters of swabs were seeded on a 15 mm 2 coverglass and dried for 30 min at 37°C to fix it. Each sample was incubated for 30 min with green and red Apt#9-QDs (2 μ L) in PBS with BSA 1% and dried at RT before being observed in the epifluorescence microscope at 400x magnification. The microscope exposition was adjusted to discard the fluorescence background of individual nanoparticles, and the positive fluorescence aggregates (yellow) sized between 2 to 5 micrometres were counted.

2.7.2 SARS-CoV-2 detection

Swab samples (50 μ L) were mixed with green and red Apt#9-QDs mixture 100 pM (10 μ L). The mixture is incubated at RT for 2 h without shaking. One and a half microliters from the bottom of the sample tube were recovered and seeded in a coverslip, dried at RT and observed in the epifluorescence microscope at 200x magnification. Serial $\frac{1}{5}$ dilutions were performed up to $\frac{1}{625}$. Yellow aggregates were counted in six homogeneous fields.

3. Results and Discussion

Bioh-QDs nanostructures with specific recognition of SARS-CoV-2 viral particles were prepared using aptamers as recognition molecules. In the first step, a design and selection of a specific aptamer from a library is required. The aptamer will be bound to the Bioh-QDs surface in the second step.

3.1 DNA-Aptamer as a recognition molecule

The interaction of DNA and proteins has been found in many essential biological processes [Jayasena, 1999]. The evolution of DNA technology in the last twenty years allows the application of these molecules as synthetic antibodies [Radrizzani et al., 2000, Bianchini et al., 2001].

An aptamer prepared from a single-stranded DNA combinatorial library is selected as a recognition molecule for the nanoconstructs. The designed aptamer applied in this work is inspired by the immunoglobulin G structure, containing a 'variable' and a 'constant' domain (Fig. 1A). The first one involves the molecular recognition of the target; meanwhile, the latter will give conformational stability to the whole molecule. The variable domain is a single-stranded DNA of 50 bases. The constant domain is assembled by two complementary sequences (13 bases each) in each extreme, forming a fork with a constant and stable double helix (Fig. 1A). Two single strands sequences (3 bases in 3' and 7 bases in 5') are additionally included as tails to add tags or as spacers for decoration of nanoparticles. These regions also contain the sequences of the primers required for aptamer amplification.

FIGURE 1

3.4 Aptamer selection

Specific aptamers are developed by an *in vitro* selection from a library prepared by chemical synthesis. Classical aptamer selection starts with a library containing 10¹⁴ different aptamer molecules. After iterative

selection/amplification cycles, a few aptamers with specificity and affinity for the target can be recovered [Tuerk and Gold, 1990]. Another modern approach uses capillary electrophoresis to select aptamers without amplification steps [Drabovich et al., 2005; Le et al., 2019]. In this assay, a PCR pre-amplified library was used to do only one selection round, as described previously [Moncalero et al., 2011]. Aptamer selection is done in solution and separated by filter binding assay [Moncalero et al., 2011; Rio, 2012]. A procedure scheme is depicted in Fig. 1B.

Receptor Binding Domain Spike protein (RBD) of the SARS-CoV-2 virus is used as antigen protein for aptamer selection. Briefly, after incubation, RBD and the protein-bound aptamers are captured by the nitrocellulose membrane and eluted. A further amplification step by PCR reaction allows the enrichment of specific aptamers from the membrane elution. To follow the aptamers, amplification was performed with a tagged 5' DNAzymes-peroxidase primer and determined by dot blot analysis [Longinotti et al., 2021].

One aptamer selection step was performed in quadruplicate to increase the probability of positive selections. A dot blot assay was used to determine the specificity of the aptamer selection for the recognition of RBD protein. Six aptamers of the most intense dot-blot library selection were cloned (Fig. 2A) and sequenced (Table S1). Antigen recognition property against RBD and SARS-CoV-2 was confirmed by dot blot analysis (Fig. S1).

The dissociation constants of the most intense dot blot clone (#9) were determined by filter binding assay yielding 20 nM (Fig. 2B and C) using the procedure described in the Supplementary Information. Meanwhile, the sensitivity of the method, using an aptamer concentration of 125 nM, was determined in 1 ng RBD, equivalent to 20 fmols (see Fig. S1).

A model 3D structure of clone #9 was modelled using prediction software. Fig. 2D are shown the three more likely structures output from 3dRNA prediction software [Zhang et al., 2022]. It is also shown the structure superposition of these three structures. All the structures share the same confirmation of the 'constant' and 'variable' regions. The seven bases corresponding to regions contiguous to primers allow a hinge movement that

resembles the hinge region of the antibodies (Fig. 2D and Supplementary Video 1).

FIGURE 2

3.5 Biohybrid QDs

A nanoconstruct (Fig. 3A) that can recognise and precisely interact with a single viral particle in a biological media requires at least two critical features, (a) the absence of nonspecific interactions with the biological media and (b) a specific and high-affinity recognition surface. The former property can be reached by a multilayer albumin coating of nanoparticles stabilised by a chemical crosslinking process. This stabilised multilayer is critical for preserving the recognition properties of the ligands attached. The chemical crosslinking process of the albumin can be performed by ionising radiation [Flores et al., 2018; Flores et al., 2019; Achilli et al., 2022] or by the combination of ultrasound energy and chemical crosslinkers [Traverso et al., 2023]. In this work, the latter procedure is selected as it is less labour-intensive.

Specific and high-affinity recognition features can be addressed by decorating the Bioh-QDs surface with recognition molecules interacting simultaneously and cooperatively with the target. In this way, affinity can be increased by the interaction of multiple binding sites. To maximise these interactions, it is mandatory that oriented immobilisation onto the QD surface. Bioh-QD decoration was performed in an oriented fashion by using the glutaraldehyde chemistry [Traverso et al., 2023]. Freshly prepared Bioh-QDs are glutaraldehyde-activated, which react with ligands containing an amino moiety, such as C6-NH₃ 5'-aptamers or RBD protein, in excess.

Bioh-QDs are characterised by UV-vis spectroscopy, electrophoretic mobility, TEM, and DLS (Fig. 3). The UV-vis measurements show the presence of proteins (280 nm peak) and the DNA content (260 nm peak) of Bioh-QDs after decoration, changing 260/280 ratios from 0.93 to 1.62 (Fig. 3B). Nanoparticle separation by electrophoresis gel (Fig. 3C) shows the aptamer

decoration onto albumin nanoparticles; QDs were omitted from the preparation to develop DNA in the nanoconstruct by EtBr without interference. Fig. 3D shows an agarose gel of red Bioh-QDs before and after the purification (Lines #1 and #3, respectively) and Apt#9-QDs before and after the purification (Lines #2 and #4, respectively) stained with FSC and EtBr simultaneously. TEM pictures show the Bioh-QDs stained with uranyl acetate of an average of 14.5 nm (Fig. 3E and S2).

DLS analysis shows a hydrodynamic diameter of 75 nm corresponding to the Apt#9-QDs (Fig. 3F), which is reduced to 20 nm after treatment with DNAse, recovering their original size of Bioh-QDs. Using the same technique is possible to measure an increment of 20 nm in the hydrodynamic diameter of Apt#9-QDs after adding free RBD antigen to the suspension (Fig. 3G).

FIGURE 3

3.2 Multiple and cooperative interactions

Multivalent interactions are universally applied to strengthen specific interactions between biological surface structures. In contrast to weak monovalent reversible binding, multivalent interactions offer the advantage of a multiple and thus dramatically enhanced binding on a molecular scale [Fasting et al., 2012]. This phenomenon is a critical principle in nature and paramount in bionanotechnology because cooperativity allows particle/particle interaction at concentrations lower than the dissociation constant of single interactions. In our case, decorated nanoconstructs with several equal recognition molecules will enhance the affinity binding to other particles containing multiple equal antigens, such as RBD-decorated Bioh-QDs or viral particles.

To demonstrate the improved recognition properties in the solution of the decorated nanoconstructs, two decorated Bioh-QDs were prepared: red Bioh-QDs decorated with RBD antigens on their surface (RBD-QDs) and green QDs decorated with aptamers (Apt#n-QDs).

The mixture of both nanoconstructs at 1 nM concentration is visualised by fluorescence microscopy after incubating at room temperature for 20 min. According to the Rayleigh criterion (see below), when a red RBD-QD binds to a green Apt#n-QD, both QDs overlay the emission wavelengths yielding a yellow emission which is observed under dual filter fluorescence microscopy.

3.3 Rayleigh's criterion

The chance for the observer to discriminate between two different particles of two different QD wavelength emissions (colours): green and red, will depend on the resolution power of the lens used (eye or microscope lens) (Fig. 4A). The maximum resolution obtained with visible light in a microscope is close to 200 nm because the shortest wavelength is close to 400 nm. To the naked eye, green and red QDs suspension are visualised as yellow. However, single QDs (green or red ones) are discriminated by visualisation at an intermediate (i.e. 100x - 200x) and high magnification (i.e. >400x); this is due to the increase in the numerical aperture, which in these cases can be increased up to about 1.25. In the particular case that the distance between two Bioh-QDs of different colours is lower than 250 nm (wavelength/2), they will be visualised as a yellow signal (Fig. 4A) under the microscope. The numerical aperture cannot achieve the required resolution. This phenomenon allows us to determine when they interact with each other. Fig. 4B shows fluorescence microscopy images of red RBD-QDs (or Bioh-QDs used as control), and green Apt-QDs mixtures. Previously, QDs mixture is dried onto a coverslip to visualise all the nanoparticles in the same focus at 1600x magnification (Fig. 4B). Mixtures corresponding to red RBD-QDs with green Apt#n-QDs (Apt#1-QDs; Apt#4-QDs; Apt#9-QDs) show yellow aggregates; meanwhile, samples prepared with red Bioh-QDs did not show any yellow aggregate. According to Fig. 4B, Apt#9-QDs showed the best interaction with RBD-QDs, confirming the results of aptamer selection (results corresponding to Apt#7-QDs; Apt#8-QDs; Apt#12-QDs are shown in Fig. S3).

3.4 SARS-CoV-2 recognition by Apt#9-QDs

As previously described, according to the Rayleigh criterion, when a green and red decorated Bioh-QDs are at <250 nm distance, the emission-wavelength overlay yields a yellow emission, independent of the magnification when it is higher than 200x. Therefore, red and green Apt#9-QDs are prepared to specifically recognise SARS-CoV-2 viral particles in swab samples to take advantage of this phenomenon.

Initially, Apt#9-QDs mixture was used to identify RBD immobilised onto a nitrocellulose membrane by a dot blot assay (Fig. 5A and B). This demonstrates that aptamers onto Apt#9-QDs surfaces preserve their recognition properties. Fig. 5A is shown the QDs fluorescence (ImageQuant LAS 500); meanwhile, Fig. 5B shows the microscopy images obtained with a 4x lens using different filters onto the same dot. Both green and red Apt#9-QDs can equally recognise RBD as expected, and non-fluorescence is found in the control dot.

Considering that Apt#9-QDs can bind multiple RBD proteins onto a single nanoconstruct (see Fig. 3A), in the following experiment, viral particles (from patient #5 swab) were used to generate aggregates by adding Apt#9-QDs. Fig. 5C shows a DLS (measured as % mass) of a SARS-CoV-2 viral sample before and after adding Apt#9-QDs. A clear shift to particle populations of 500 nm and one micron was found. On the same sample, free RBD protein was added previously to Apt#9-QDs. In this case, one-micron aggregates are absent and only 500-nm-aggregate was found (Fig. 5C). The specificity of the interaction is demonstrated by the presence of RBD protein in the reaction mixture, which acts as a competitor. In addition, it is remarkable that RBD only compete with the major aggregates and non with SARS-CoV-2/Apt#9-QDs complexes.

To visualise the SARS-CoV-2/Apt#9-QDs interaction, patient#5 swab sample ($1.5 \,\mu L$) was previously fixed to $15 \,mm^2$ microwell onto a coverslip (see Fig. S4) by air drying process; in a second step, green and red Apt#9-QDs are added and dried in the micro-well. No washes were required, and direct microscope visualisation was performed. The high hydrophilicity of Bioh-QDs avoids particle aggregation at the air/liquid interface of the drop; therefore,

non-interacting Apt#9-QDs are visualised as single particles (green and red ones) after drying (see Fig. 5D). Meanwhile, in the presence of SARS-CoV-2 viral particles yellow aggregates are visualised by not complying with the Rayleigh criterion. Also, the size of the final particle will be larger than the original virus particle as DLS measures it (Fig. 5C), improving their recognition at lower microscopy magnification and, in this way, enhancing the difference between interacting and non-interacting Apt#9-QDs.

Microscopy analysis of the negative microwell shows only four yellow aggregates versus 186 found in the positive microwell, from 1.2×10^9 Apt#9-QDs added in each one. Every yellow signal corresponds to a single viral particle surrounded by several green and red Apt#9-QDs; which are visualised as yellow because they are at <250 nm distance. This quantification corresponds to 1.2×10^5 viral particles/swab mL (186 particles/1.5 μ L). This value is below the average viral load for swabbing techniques during the first 5 days of infection (6.76 \times 10⁵ copies per swab) [Pan et al.,2020].

FIGURE 5

3.4 SARS-CoV-2 detection in swab samples

Considering the virus particle and Apt#9-QDs sizes, it is expected that a SARS-CoV-2/Apt#9-QDs complex could have between six and twelve Apt#9-QDs per virion, reaching a particle of 500-nm size. However, in solution bigger aggregates can be found (see Fig. 5C). Taking into account this aggregation property it is proposed to create a very sensitive SARS-CoV-2 viral detection method using patient swabs.

Patient#5 swab (50 μ L) were mixed with green and red Apt#9-QDs (10 μ L). After incubation at RT for 2 h for seating down the macroaggregates, 1.5 μ L from the sediment are seeded in a coverslip. In Fig. 6 are compared microscopy images of the same patient swab: fixed sample at 400x magnification (Fig. 6B) and the sediment collected, where well-defined yellow macroaggregates are easily visualised at 200x magnification (N= 96) (Fig. 6C). Considering all viral particles are in the 96 aggregates, at least an average of

60 viral particles per aggregate (1.2 x 10^5 viral * 50 μ L/ 1000 μ L/ 96) can be estimated.

In order to estimate the sensitivity of the method, patient#5 swab sample was serially diluted $\frac{1}{5}$ up to $\frac{1}{625}$ and incubated with Apt#9-QDs (Fig. S7). Yellow particles could be found in up to $\frac{1}{125}$ dilution, considering this sample as positive (1.2×10^5 viral particles/swab mL); which means that they can be found around 50 viral particles per sample ($50 \mu L$).

A total of 12 patient swabs without dilution were analysed (6 positives and 6 negatives), reaching a result in accordance with the lateral flow test (Fig. S5 and S6).

FIGURE 6

4. Conclusions

Using a wide-field fluorescence microscope, a straightforward application of Apt-QDs to recognise SARS-CoV-2 viral particles in swab samples is performed. Decorated Bioh-QDs of small/medium size are prepared with improved solubility, low nonspecific protein adsorption and specific recognition properties reached by aptamers.

From the six clones selected from the library, Apt#9 was chosen based on the experimental results. In addition, Apt-QDs decorated with this clone show a magnified SARS-CoV-2 viral interaction by homo-multivalent interactions, which are not fully reversed by free RBD protein addition as expected.

It demonstrated SARS-CoV-2/Apt#9-QDs interaction using two fluorescence emissions (green and red) Apt#9-QDs with equal recognition properties. An overlap of the wavelength emissions observed means that these particles are interacting at shorter distances than the Rayleigh criterion. In addition, the increment in the particle diameter by aggregation enhances particle recognition by fluorescence microscopy at 200x magnification.

A very sensitive and simple procedure is proposed for SARS-CoV-2 viral detection in swab samples. It has two main advantages, generation of macroaggregates, which can easily settle down, concentrating viral particles and generating macroaggregates, which increases the fluorescence emission with a concomitant change in the wavelength of the emitted fluorescence, simplifying their recognition by fluorescence microscope.

It is envisioned that this procedure, which does not require enzymatic amplification, washing and separation steps, could be compared with PCR assay sensibility.

Acknowledgements

We thank Nicolas Bruni for their chemical technical assistance, "Hemoderivados Cordoba" for the HSA and ECyT UNSAM for the support provided. This work was funded by the Ministry of Science, Technology and Productive Innovation (MIN-CYT) grant PICT 2017-0852 and PICT-startup 2021-0018 and PUNQ BIONATLP 827- 2272/22 (Universidad Nacional de Quilmes).

Supplementary Materials: The following supporting information can be downloaded at: xxxxxxxxxx

Video S1: 3D view of structure superposition of the three simulated aptamer #9 structures.

Author Contributions: Conceptualization, M.R. and M.G.; methodology, M.R., C.Y.F., J.S., O.G., C.D., A.C. and L.J.M.H.; data curation, J.S., O.G., C.D., A.C. and L.J.M.H.; validation, M.R., C.Y.F., C.P. and M.G.; formal analysis, M.R., C.P. and M.G.; investigation, M.R., J.S.Y. and M.G.; resources, M.R. and M.G.; visualization, M.G. and M.R.; supervision, M.G. and M.R.; writing—original draft preparation, M.R. and M.G.; writing—review and editing, M.R., J.S.Y., C.P. and M.G.; project administration, M.G. and M.R.; funding acquisition, M.G. and M.R.

All authors have read and agreed to the published version of the manuscript.

Conflicts of Interest: The authors declare no conflict of interest.

References

Achilli, E., Flores, C.Y., Temprana, C.F., Alonso, S.D.V., Radrizzani, M. and Grasselli, M., 2022. Enhanced gold nanoparticle-tumor cell recognition by albumin multilayer coating. *OpenNano*, 6, p.100033. DOI: 10.1016/j.onano.2021.100033

Agrawal, A., Zhang, C., Byassee, T., Tripp, R.A. and Nie, S., 2006. Counting single native biomolecules and intact viruses with color-coded nanoparticles. *Analytical chemistry*, 78(4), pp.1061-1070. DOI: 10.1021/ac051801t

Almendral-Parra, M.J., Alonso-Mateos, A., Boyero-Benito, J.F., Sánchez-Paradinas, S. and Rodríguez-Fernández, E., 2014. A novel approach to the fabrication of CdSe quantum dots in aqueous solution: procedures for controlling size, fluorescence intensity, and stability over time. *Journal of Nanomaterials*, *2014*, pp.5-5. DOI: 10.1155/2014/397469

Betancor, L., López-Gallego, F., Hidalgo, A., Alonso-Morales, N., Mateo, G.D.O.C., Fernández-Lafuente, R. and Guisán, J.M., 2006. Different mechanisms of protein immobilization on glutaraldehyde activated supports: effect of support activation and immobilization conditions. *Enzyme and microbial technology*, *39*(4), pp.877-882. DOI: 10.1016/j.enzmictec.2006.01.014

Bianchini, M., Radrizzani, M., Brocardo, M.G., Reyes, G.B., Solveyra, C.G. and Santa-Coloma, T.A., 2001. Specific oligobodies against ERK-2 that recognize both the native and the denatured state of the protein. *Journal of immunological methods*, *252*(1-2), pp.191-197. DOI: 10.1016/S0022-1759(01)00350-7

Chakraborty, B., Das, S., Gupta, A., Xiong, Y., TV, V., Kizer, M.E., Duan, J., Chandrasekaran, A.R. and Wang, X., 2022. Aptamers for viral detection and inhibition. *ACS Infectious Diseases*, *8*(4), pp.667-692. DOI: 10.1021/acsinfecdis.1c00546

Drabovich, A., Berezovski, M. and Krylov, S.N., 2005. Selection of smart aptamers by equilibrium capillary electrophoresis of equilibrium mixtures (ECEEM). Journal of the American Chemical Society, 127(32), pp.11224-11225. DOI: 10.1021/ja0530016

Ellington, A.D. and Szostak, J.W., 1990. In vitro selection of RNA molecules that bind specific ligands. *nature*, *346*(6287), pp.818-822.

Fasting, C., Schalley, C.A., Weber, M., Seitz, O., Hecht, S., Koksch, B., Dernedde, J., Graf, C., Knapp, E.W. and Haag, R., 2012. Multivalency as a chemical organization and action principle. *Angewandte Chemie International Edition*, *51*(42), pp.10472-10498. DOI: 10.1002/anie.201201114

Flores, C.Y., Achilli, E. and Grasselli, M., 2018. Radiation-induced preparation of core/shell gold/albumin nanoparticles. *Radiation physics and chemistry*, *142*, pp.60-64.

Flores, C.Y., Achilli, E., Schinca, D.C. and Grasselli, M., 2019. Plasmon properties of multilayer albumin/gold hybrid nanoparticles. *Materials Research Express*, *6*(5), p.055005.

- Jayasena, S.D., 1999. Aptamers: an emerging class of molecules that rival antibodies in diagnostics. *Clinical chemistry*, *45*(9), pp.1628-1650.
- Hu, J., Wang, Z.Y., Li, C.C. and Zhang, C.Y., 2017. Advances in single quantum dot-based nanosensors. *Chemical Communications*, *53*(100), pp.13284-13295. DOI: 10.1039/C7CC07752A
- Le, A.T., Krylova, S.M., Kanoatov, M., Desai, S. and Krylov, S.N., 2019. Ideal- Filter Capillary Electrophoresis (IFCE) Facilitates the One- Step Selection of Aptamers. *Angewandte Chemie*, 131(9), pp.2765-2769. DOI: 10.1002/anie.201812974
- Lee, J.F., Stovall, G.M. and Ellington, A.D., 2006. Aptamer therapeutics advance. *Current opinion in chemical biology*, 10(3), pp.282-289. DOI: 10.1093/clinchem/45.9.1628
- Li, H., Zhou, D., Browne, H., Balasubramanian, S. and Klenerman, D., 2004. Molecule by molecule direct and quantitative counting of antibody-protein complexes in solution. *Analytical chemistry*, 76(15), pp.4446-4451. DOI: 10.1021/ac049512c
- Liu, X., Huang, C., Zong, C., Liang, A., Wu, Z., Zhang, Y., Zhang, Q., Zhao, W. and Gai, H., 2018. A Single-Molecule Homogeneous Immunoassay by Counting Spatially "Overlapping" Two-Color Quantum Dots with Wide-Field Fluorescence Microscopy. *ACS sensors*, *3*(12), pp.2644-2650. DOI: 10.1021/acssensors.8b01092
- Longinotti, G., Ybarra, G., Vighi, S., Perandones, C., Montserrat, J., Yakisich, J.S., Grasselli, M. and Radrizzani, M., 2021. One-step histological detection and staining of the PTEN tumor suppressor protein by a single-strand DNA. Diagnostics, 11(2), p.171. DOI: 10.3390/diagnostics11020171
- Moncalero, V.L., Costanzo, R.V., Perandones, C. and Radrizzani, M., 2011. Different conformations of phosphatase and tensin homolog, deleted on chromosome 10 (PTEN) protein within the nucleus and cytoplasm of neurons. *PLoS One*, *6*(4), p.e18857. DOI: 10.1371/journal.pone.0018857
- Noseda, D.G., D'Alessio, C., Santos, J., Idrovo-Hidalgo, T., Pignataro, F., Wetzler, D.E., Gentili, H., Nadra, A.D., Roman, E., Paván, C. and Ruberto, L.A., 2023. Development of a Cost-Effective Process for the Heterologous Production of SARS-CoV-2 Spike Receptor Binding Domain Using Pichia pastoris in Stirred-Tank Bioreactor. *Fermentation*, *9*(6), p.497. DOI: 10.3390/fermentation9060497
- Nguyen, N.N.T.; McCarthy, C.; Lantigua, D.; Camci-Unal, G. Development of Diagnostic Tests for Detection of SARS-CoV-2. Diagnostics 2020, 10, 905. DOI: 10.3390/diagnostics10110905
- Pan, Y.; Zhang, D.; Yang, P.; Poon, L.L.M.; Wang, Q. Viral load of SARS-CoV-2 in clinical samples. Lancet Infect. Dis. 2020, 20, 411–412. DOI: 10.1016/S1473-3099(20)30113-4
- Radrizzani, M., Brocardo, M.G., Solveyra, C.G., Bianchini, M., Reyes, G.B., Cafferata, E.G., Ortiz, G.V. and Santa-Coloma, T.A., 2000. Development of monoclonal oligobodies and chemically synthetized oligobodies. *MEDICINA-BUENOS AIRES-*, *60*, pp.55-60. DOI:
- Rio, D.C., 2012. Filter-binding assay for analysis of RNA-protein interactions. *Cold Spring Harbor Protocols*, 2012(10), pp.pdb-prot071449. DOI: 10.1101/pdb.prot071449
- Song, Y., Zhang, Y. and Wang, T.H., 2013. Single quantum dot analysis enables multiplexed point mutation detection by gap ligase chain reaction. *Small*, *9*(7), pp.1096-1105. DOI: 10.1002/smll.201202242
- Traverso, A.N., Fragale, D.J., Viale, D.L., Garate, O., Torres, P., Valverde, G., Berra, A., Torbidoni, A.V., Yakisich, J.S., Grasselli, M. and Radrizzani, M., 2023. Two-Step Preparation of Protein-Decorated Biohybrid Quantum Dot Nanoparticles for Cellular Uptake. *Pharmaceutics*, *15*(6), p.1651. DOI: 10.3390/pharmaceutics15061651

Tuerk, C. and Gold, L., 1990. Systematic evolution of ligands by exponential enrichment: RNA ligands to bacteriophage T4 DNA polymerase. *science*, *249*(4968), pp.505-510

Tyrakowski, C.M. and Snee, P.T., 2014. A primer on the synthesis, water-solubilization, and functionalization of quantum dots, their use as biological sensing agents, and present status. *Physical Chemistry Chemical Physics*, *16*(3), pp.837-855. DOI: 10.1039/c3cp53502a

Wiberg, F.C., Rasmussen, S.K., Frandsen, T.P., Rasmussen, L.K., Tengbjerg, K., Coljee, V.W., Sharon, J., Yang, C.Y., Bregenholt, S., Nielsen, L.S. and Haurum, J.S., 2006. Production of target-specific recombinant human polyclonal antibodies in mammalian cells. *Biotechnology and bioengineering*, *94*(2), pp.396-405. DOI: 10.1002/bit.20865

Woloshin, S., Patel, N. and Kesselheim, A.S., 2020. False negative tests for SARS-CoV-2 infection—challenges and implications. New England Journal of Medicine, 383(6), p.e38. DOI: 10.1056/NEJMp2015897

Zhang, Q., Li, J., Pan, X., Liu, X. and Gai, H., 2021. Low-numerical aperture microscope objective boosted by liquid-immersed dielectric microspheres for quantum dot-based digital immunoassays. *Analytical Chemistry*, *93*(38), pp.12848-12853. DOI: 10.1021/acs.analchem.1c02709

Zhang, Y., Wang, J. and Xiao, Y., 2022. 3dRNA: 3D structure prediction from linear to circular RNAs. *Journal of Molecular Biology*, *434*(11), p.167452.DOI: 10.1016/j.jmb.2022.167452

Zhou, J., Zuo, Y., Wan, X., Long, G., Zhang, Q., Ni, W., Liu, Y., Li, Z., He, G., Li, C. and Kan, B., 2013. Solution-processed and high-performance organic solar cells using small molecules with a benzodithiophene unit. *Journal of the American Chemical Society*, *135*(23), pp.8484-8487. DOI: 10.1021/ja3110329

FIGURES

Figure 1: (A) Scheme of aptamer used for antigen recognition; (B) scheme of filter binding assay applied to the aptamer selection from a library.

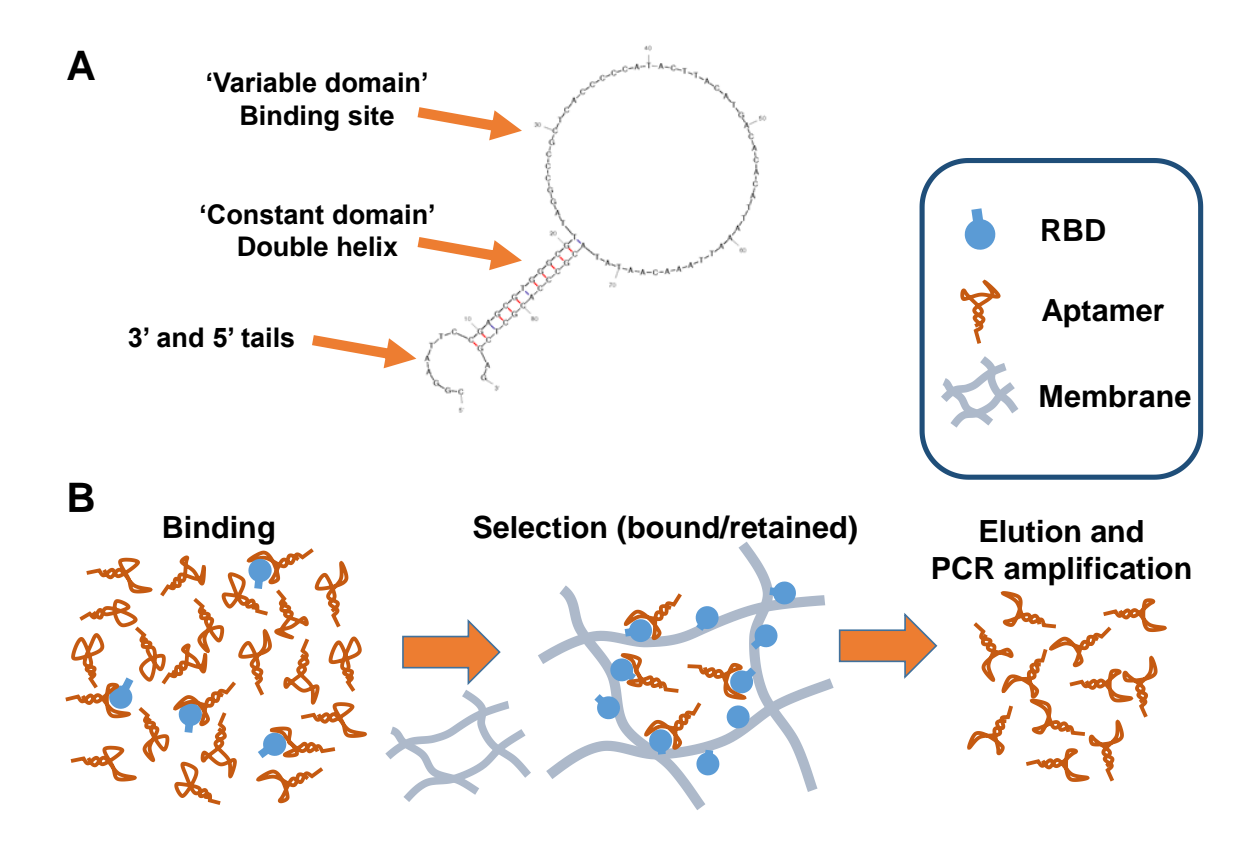


Figure 2: (A) Dot blot assay of RBD developed with luminol onto aptamer clones labeled with DNAzymes peroxidase; (B) filter binding assay to determine the dissociation constant of clone #9; (C) Plot of signal intensity of RBD/Apt#9 versus RBD concentration; (D) 3D pictures of most likely conformers of Apt#9 and their superposition according to 3dRNA software.

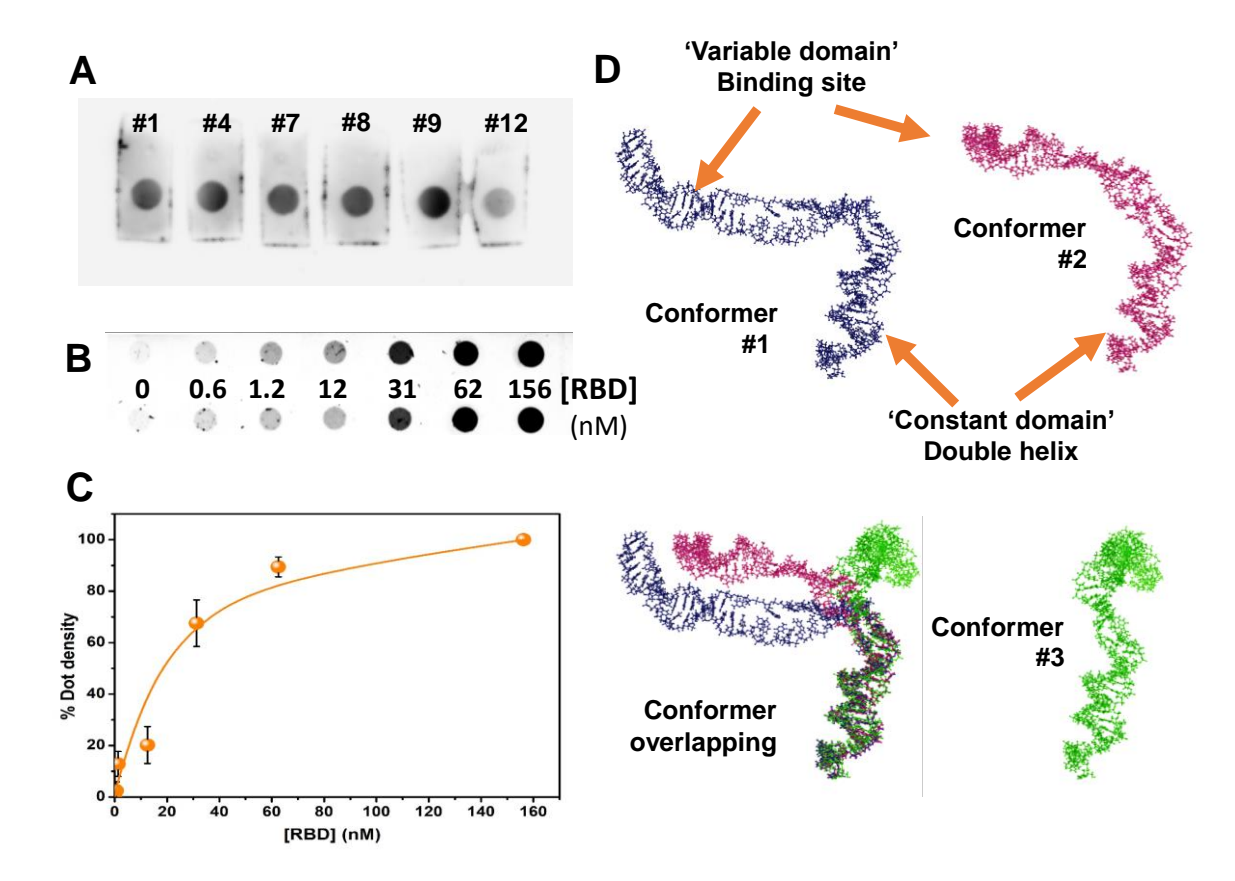


Figure 3: (A) Scheme of decorated Bioh-QDs (Apt-QDs); (B) UV-vis spectra of Bioh-QDs and Apt-QDs; (C) Agarose electrophoresis: lane #1: albumin (FSC stain); lane #2: albumin nanoparticle (FSC stain); line #3: Apt#9 (BrEt stain); line #4: Ap#9-albumin nanoparticle (BrEt stain); (D) Agarose electrophoresis stained with FSC and BrEt: line #1: Bioh-QDs without purification; line #2: Apt#9-QDs without purification; line #3: purified Bioh-QDs; line #4: purified Apt#9-QDs; (E) TEM picture of Bioh-QDs; (F) DLS of Apt#9-QDs and Apt#9-QDs treated with DNAse and Tween-20 0.1%; (G) DLS of Apt#9-QDs and Apt#9-QDs + RBD protein.

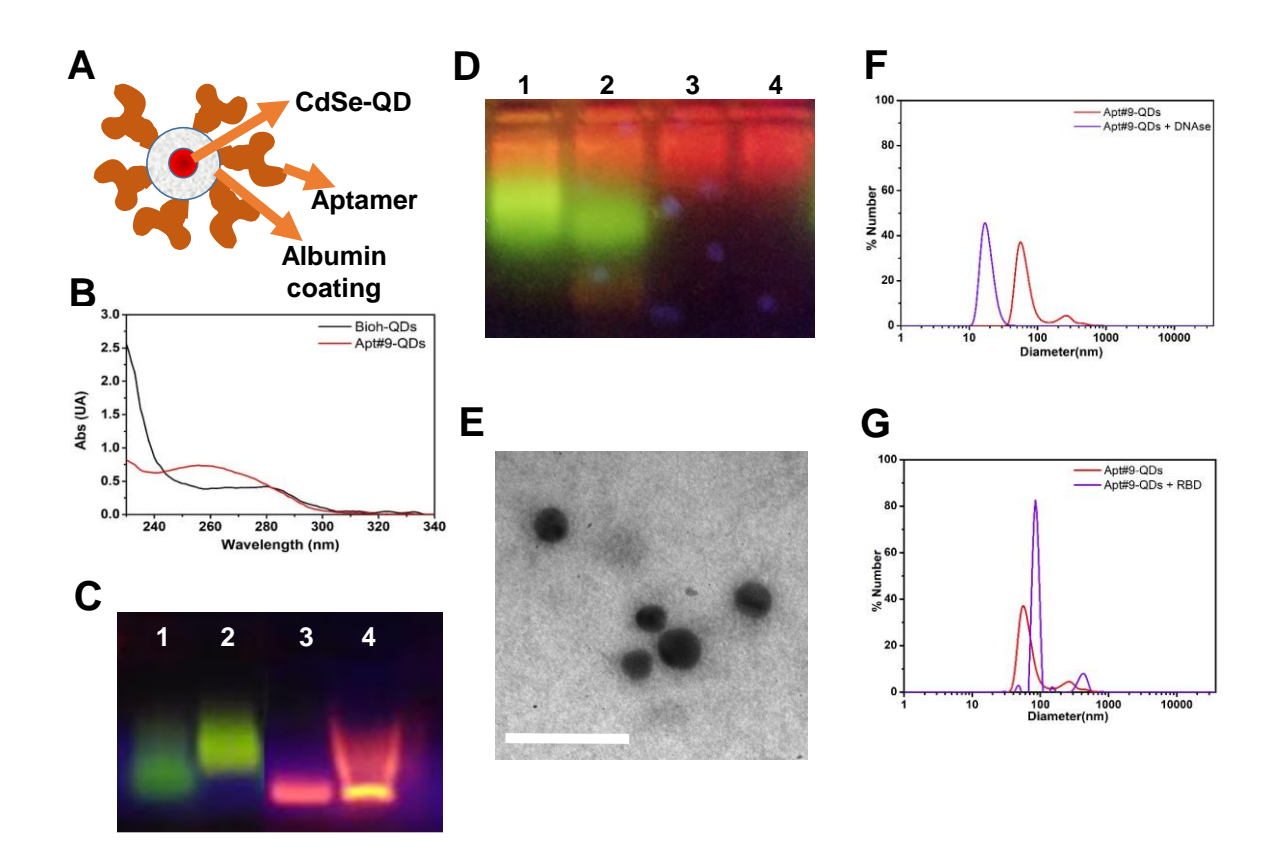


Figure 4: (A) Rayleigh criterion: green and red decorated Bioh-QDs at longer distances than 250 nm yield separated emission wavelengths. Distance between them shorter than 250 nm reaches emissions overlap; (B) Microscopy images (1,600x) of green Apt#n-QDs (#1, #4, #9) with red Bioh-QDs (control) or red RBD-QDs mixtures. Scale bar: 2 μ m.

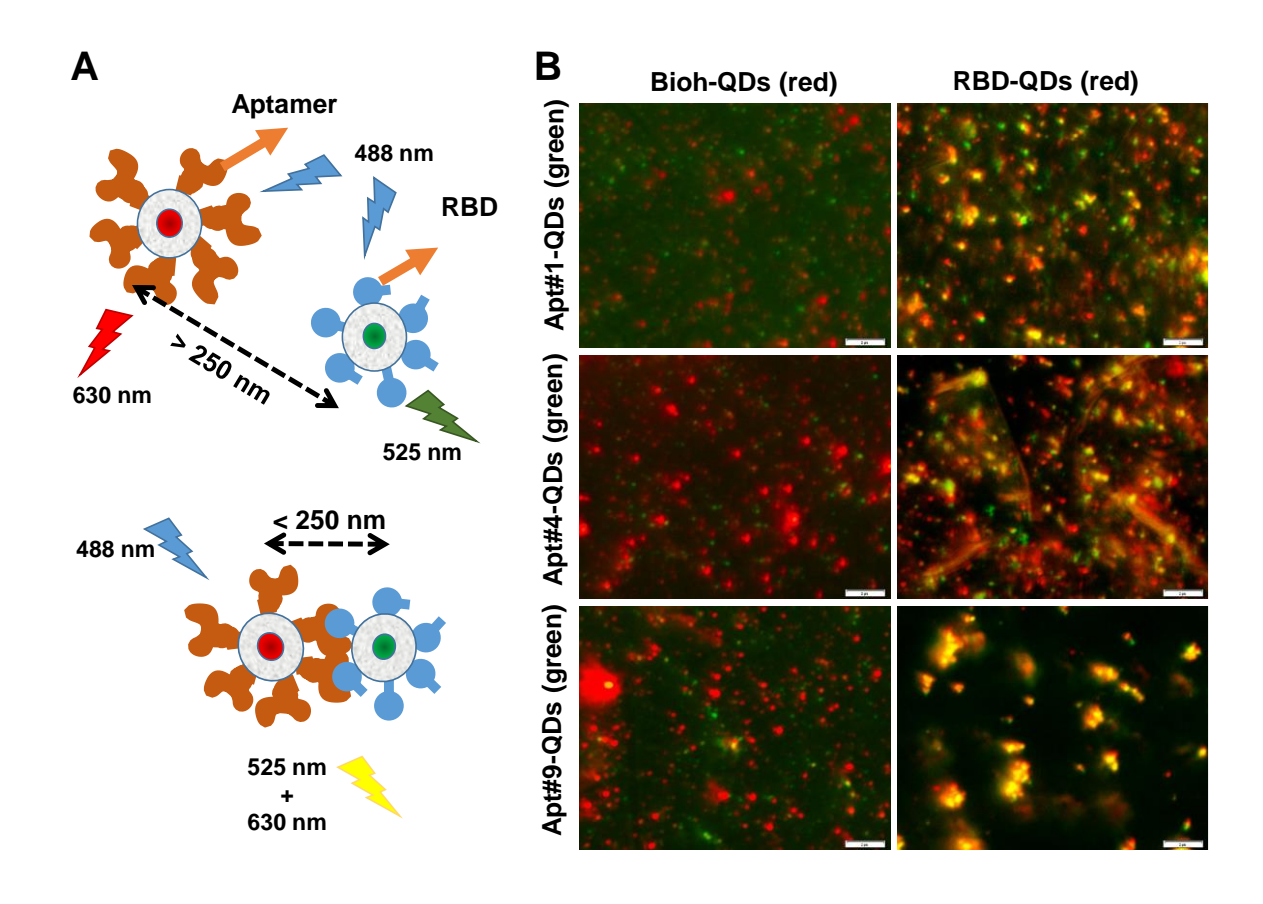


Figure 5: (A) Dot blot of RBD developed with green and red Apt#9-QDs (captured by Lass500); (B) the same dot blot membrane visualizes with 4x lens in the fluorescence microscope using different filters (488 nm, 543 nm and 488/543 nm). Serum proteins were used as control; (C) DLS of SARS-CoV-2 viral particles from patient #5 swab, viral particles + Apt#9-QDs and viral particles + Apt#9-QDs + RBD protein; (D) Microscopy images (400x) of (-) green and red Apt#9-QDs mixtures and (+) fixed SARS-CoV-2 viral particles + green and red Apt#9-QDs mixtures. Scale bar: 50 μm.

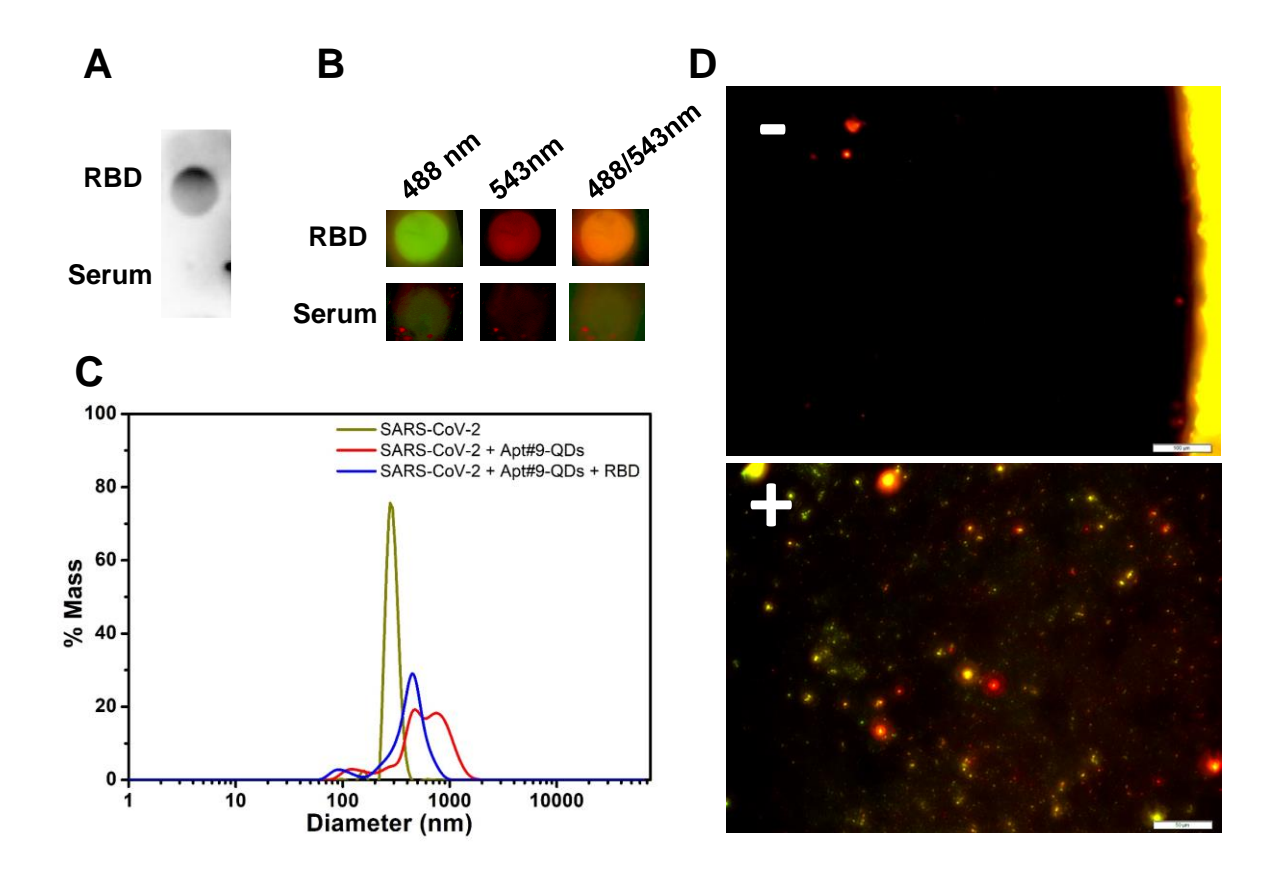


Figure 6: Fluorescence microscope images corresponding to four of six fields of (A) Apt#9-QDs without viruses (200x); (B) fixed SARS-CoV-2 viral particles from a patient#5 swab (1.5 μ L) incubated with Apt#9-QDs (400x); and (C) pellet corresponding to the same swab (50 μ L) using the proposed detection method (200x). Scale bar in (A) and (C): 100 μ m. Scale bar in (B): 50 μ m.

